

Time-domain analysis of electronic spectra in superfluid ^4He

J. Eloranta ^{a,*}, H.Ye. Seferyan ^b, V.A. Apkarian ^b

^a *Department of Chemistry, University of Jyväskylä, Surfontie 9, 40500 Jyväskylä, Finland*

^b *Department of Chemistry, University of California, Irvine, CA 92697, USA*

Received 7 June 2004; in final form 18 July 2004

Abstract

Electronic absorption spectra of impurities in superfluid helium is developed in time domain, using time-dependent density functional theory to describe liquid ^4He and time-dependent perturbation theory to describe the electronic degrees of freedom of the impurity. Angularly isotropic potentials are used to describe the molecule–helium interactions in the ground and excited electronic states. The calculations rationalize experimentally observed phonon side-bands in ^4He droplets and in bulk helium, and allow assignments of spectral features to specific motions of the liquid.

© 2004 Elsevier B.V. All rights reserved.

1. Introduction

Optical absorption spectroscopy of atoms and molecules has been successfully implemented in both superfluid helium droplets [1] and in bulk helium [2]. Of particular interest is the case of weak electron–phonon coupling, where the observed phonon side-bands accompanying a sharp zero-phonon line interrogate the elementary excitations of the fluid [3–6]. The absorption spectrum of glyoxal in helium droplets is prototypical [3]. A sharp zero-phonon line defines the electronic origin of the $S_1 \leftarrow S_0$ transition, followed by a +6 K spectral gap, and phonon wings with two broad maxima at ca. +8 and +14 K. Depending on the molecule, the gap region contains a number of additional sharp lines. Similar spectral features can be identified in bulk helium, but with much lower spectral resolution. The observed band gap and phonon wings have been explained as a reflection of the superfluid density of states. The close agreement of the spectral peaks with the maxima in the density of states of superfluid ^4He –

the maxon at $k = 1.1 \text{ \AA}^{-1}$, $E = 13.8 \text{ K}$ and the roton minimum at $k = 1.9 \text{ \AA}^{-1}$, $E = 9.1 \text{ K}$ in the bulk – is taken as evidence of the superfluidity of the doped droplet [3]. The discrete lines within the gap have been assigned either to unresolved guest rotations, or to tightly bound molecule–helium configurations [7,8]. This frequency domain interpretation does not elucidate the mechanism of coupling between chromophore and elementary excitations – phonons and rotons. A more direct connection between spectral features and their underlying microscopic dynamics is sought through the time-dependent analysis, which we report in this letter. The method relies on time-dependent density functional theory (TDFT) which we previously introduced to describe dynamics of the solvated electron in superfluid helium [9], and it takes advantage of the previously well-calibrated density functionals [10,11].

2. System and method

We consider a system with two electronic levels, which adiabatically follow the slowly varying time-dependent potential that arises from the electron–liquid interaction. Due to the large separation between the

* Corresponding author.

E-mail address: eloranta@cc.jyu.fi (J. Eloranta).

electronic levels, the bath modes cannot drive any system transitions (T_1 processes are absent). The interaction potential in both ground and excited electronic states is taken to be angularly isotropic. This reduces the treatment to a 1-D problem, where the TDFT equations can be efficiently evaluated numerically using spherical coordinates. The calculations assume bulk helium ($\rho_0 = 0.0218360 \text{ \AA}^{-3}$), initially at 0 K. We use a 2500 point spatial grid, covering $r = 3\text{--}500 \text{ \AA}$, and a total simulation length of 200 ps with 1 fs time steps (for details, see [9,12]). We will consider both bulk helium, as well as small ($N = 6000$) and large ($N = 20000$) helium droplets. This size range precludes the direct implementation of three dimensional TDFT methods, which were recently introduced [12,13].

In the standard perturbative limit of a dipolar transition, in a weak electric field, the first-order polarization, $P^{(1)}(t)$, induced with unit field strength, in the rotating frame approximation, reduces to

$$P^{(1)}(t) = \langle \psi^{(0)}(t) | \mu | \psi^{(1)}(t) \rangle + C.C. \\ \propto i \int_0^t \exp\left(-\frac{i}{\hbar} \int_{t''}^t E_{\text{ext}}(t'') dt'' - i\omega t'\right) dt' + C.C., \quad (1)$$

where μ is the dipole transition operator; and $E_{\text{ext}}(t)$ is the difference in the molecule-bath interaction energy between excited and ground electronic states

$$E_{\text{ext}}(t) = \int \rho_{\text{He}}^e(R, t) V_e(R) d^3R - \int \rho_{\text{He}}^g(R) V_g(R) d^3R, \quad (2)$$

where V_e and V_g are the excited and ground state molecule-He pair-potentials, and ρ_{He} refers to the time-dependent liquid ^4He density on either the excited (e) or ground (g) state potential. Note that Eq. (2) can be directly obtained from the TDDFT calculation. The absorption spectrum is then obtained through Fourier transform of the time-dependent polarization (1). The evaluation of the resulting expression is rather cumbersome. Instead, we analyze the power spectrum obtained from the discrete Fourier transform of $E_{\text{ext}}(t)$, using the Hanning window function. This procedure correctly

yields the phonon spectrum and allows the identification of spectral features in terms of dynamical recursions in the liquid density. However, the extracted lineshapes are not exact and overtones of resonances are not included. We note that the commonly used Anderson expression [14,15] for lineshapes in terms of static potentials, makes the questionable assumptions of instant dephasing and over-damped liquid dynamics. We try to understand the mechanics of these processes.

The essential physics sought is obtained using an exponential-6 potential to describe the molecule-helium interaction

$$V(r) = a_1 e^{-a_2(r-a_3-A_1)} - \frac{A_2 a_4}{r^6}. \quad (3)$$

The values of the parameters used to model ground and excited state combinations are shown in Table 1. The equilibrium liquid density in the ground state is plotted in Fig. 1 for the case of a strictly repulsive potential (R1–R4 in Table 1), and for the case of van der Waals binding (B6 in Table 1). In the latter case, the first shell of the liquid is strongly localized in the potential well which has a depth of 19 K at 5.7 \AA . This binding energy is slightly less than what has been estimated for a glyoxal molecule ($\sim 30\text{--}60$ K, depending on geometry) [3]. The position of the minimum is nearly that of the rotationally averaged glyoxal-helium interaction [16,17]. Detailed descriptions of liquid structure around a variety of molecular centers can be found in [15].

3. Results and discussion

Dynamics of the liquid in the excited state is followed after suddenly switching the potential parameters A_1 and A_2 (see Table 1). Snapshots of the ensuing liquid density on the repulsive R4 potential are shown in the upper panel of Fig. 2. The profiles illustrate the two characteristic motions: the fast liquid response is limited to interfacial compression ($t < 7$ ps); and the slow motion corresponds to the breathing of the bubble ($t > 7$ ps). Increasing the initial bubble radius (E5 in Table 1) merely changed the bubble breathing time with no other apparent changes

Table 1
Parameters for the applied potentials are shown (see Eq. (3))

Potential	a_1 (K)	a_2 (\AA^{-1})	a_3 (\AA)	a_4 (K \AA^6)	A_1 (\AA)	A_2 (\AA)	$R_{b,\text{ini}}$ (\AA)
R1	3.8003×10^5	1.6245	0	0	0.05	1	7.5
R2	3.8003×10^5	1.6245	0	0	0.1	1	7.5
R3	3.8003×10^5	1.6245	0	0	0.2	1	7.5
R4	3.8003×10^5	1.6245	0	0	0.6	1	7.5
E5	3.8003×10^5	1.6245	2.0	0	0.2	1	9.7
B6	3.8003×10^5	1.6245	0	1.8921×10^6	0	0.9	~ 5

For initial states $A_1 = 0$ and $A_2 = 1$ and the corresponding excited state is obtained with the A_1 and A_2 values indicated in the table.

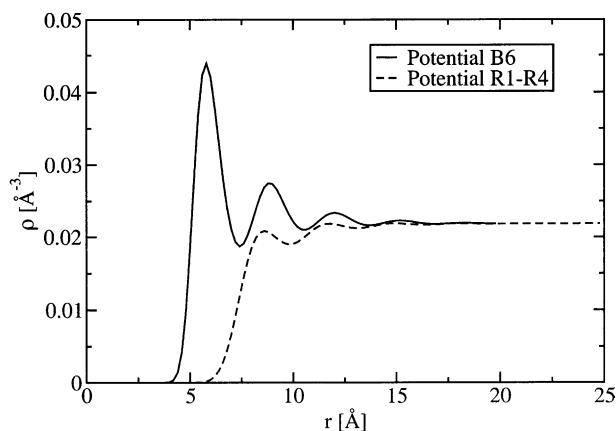


Fig. 1. Ground state liquid structures around the purely repulsive and van der Waals bound molecules are shown (R1–R4 and B6 in Table 1).

in dynamics. When van der Waals binding is present (B6 in Table 1), great enhancement in the interfacial dynamics is observed with essentially no coupling to the breathing motion. These characteristic bubble motions in bulk helium have been discussed in some detail previously [9]. In the case of droplets, additional dynamics occurs due to the liquid–vacuum boundary. When the excitations reach the boundary, both reflection and evaporation occur. Evaporation in an S-wave is illustrated in the lower panel of Fig. 2. Although the density functional could in principle allow for fractional He atom evaporation, in this case, the integrated density approximately corresponds to a single He atom.

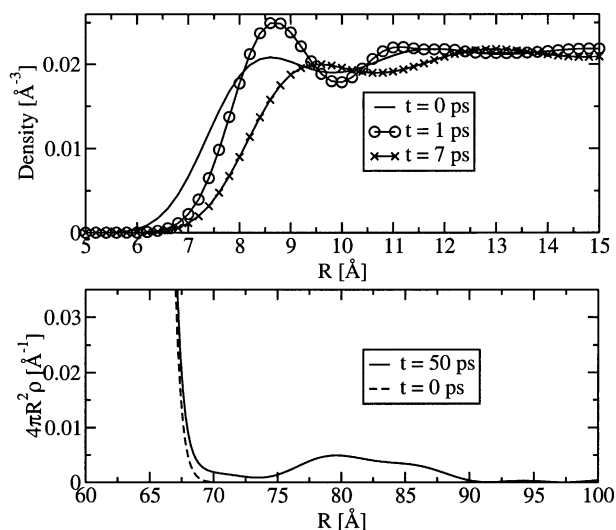


Fig. 2. Snapshots of liquid density at given times during the liquid dynamics is shown in the upper panel. At short times ($t < 7$ ps) rapid interfacial dynamics occurs and at later times $t \geq 7$ ps slower liquid breathing dynamics occurs. To demonstrate the effect, calculation was carried out for the case of R4 in Table 1. The lower panel demonstrates the quantum evaporation process from the surface of the droplet ($N = 20000$ with B6 potential).

The absorption spectrum for purely repulsive potentials (e.g. R1–R4 of Table 1) in bulk helium is shown in Fig. 3. The breathing mode leads to the absorption near 2 K. Increasing the bubble radius (E5 in Table 1) leads to a longer breathing period, and accordingly shifts the absorption closer to the zero-phonon line. Increasing the external pressure blue shifts this resonance [9], and the peak can be expected to split when the spherical symmetry of the liquid motion is broken due to anisotropy in the molecule–helium interaction. The interfacial compression mode leads to the weak spectral component at +9 K.

When van der Waals binding is included (B6 in Table 1), the spectrum in bulk helium changes dramatically, as shown in Fig. 4. The bubble breathing mode is now absent, the +9 K component gains intensity, a new line appears at +14 K along with a smaller broad shoulder at +16 K. The van der Waals well localizes the liquid, prevents the large amplitude breathing motion, and generates a shell structure that can be identified by the deeply modulated static density shown in Fig. 1. The observed sidebands are now strictly due to persistent interfacial excitations arising from oscillations of the solvent shells in the bound potential, namely, the localized excitations. The frequencies of the persistent localized excitations, at 9 and 14 K, coincide with the energies of the maxon and roton minimum built-in the density functional. To ascertain that this is not a coincidence, we have repeated the same simulations using the density functional of Dupont-Roc et al. [18], in which the extrema in the dispersion curve are systematically blue shifted. The observed phonon side-bands faithfully track this shift. In essence, the impulsive preparation drives the full spectrum of elementary excitations in the liquid.

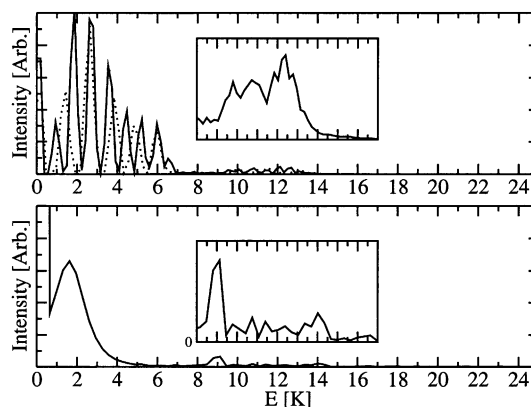


Fig. 3. Absorption spectra for purely repulsive interaction (R3 in Table 1) are shown with the zero phonon line located at 0 K. The upper panel displays spectra for helium droplets with $N = 20000$ (solid line) and $N = 6000$ (dashed line) and the lower panel shows the corresponding bulk helium spectrum. The insets show magnification of the given spectral region.

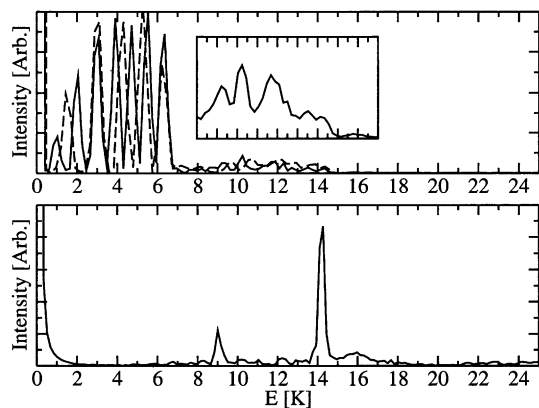


Fig. 4. Absorption spectra for van der Waals bound molecules are shown (B6 in Table 1) with the zero phonon line located at 0 K. The upper panel displays spectra for helium droplets with $N = 20000$ (solid line) and $N = 6000$ (dashed line) and the lower panel shows the corresponding bulk helium spectrum. The inset shows magnification of the given spectral region.

However, the local modes that persist are those at the extrema in the dispersion curve, where the group velocity drops to zero allowing localization.

The spectra in the finite size helium droplets are distinctly different from those of the bulk, as seen in Figs. 3 and 4. In comparison with the bulk spectra, the maxon and roton resonances are smeared out in the droplets. The droplet spectra are dominated by the oscillations of the liquid shell bounded by the molecule-liquid and liquid-gas interfaces. The motion generates a regular progression between the zero-phonon line and ~ 7 K, the upper limit being determined by quantum evaporation. The observed fundamental frequencies are 1.5 K in the 6000 atom droplet and 1.0 K in the 20000 atom droplet. These simply correspond to the fundamental shell oscillation frequencies: $\omega = 2\pi v/2d$, where $v = 220$ m/s is the velocity of sound in helium, and d is the thickness of the liquid shell around the molecule ($d = 35$ and 55 Å in the small and large droplets, respectively). The regular recursions of the density packet to the bubble edge, after being reflected at the droplet wall, modulate the electronic energy and yield the observable spectrum. A progression, as opposed to a single line, arises because the temporal width of the density packet at the turning points is short in comparison to the recursion period. These sharp resonances, however, are peculiar to a molecule located at the center of the droplet, which is imposed by the one-dimensional treatment. In practice, at the characteristic temperature of droplet experiments of 0.39 K, the soft trapping potential leads to a distribution in the eccentricity of the molecule, with vanishingly small probability of finding a molecule at the center [19,20]. To compare to experiments, in addition to the eccentricity distribution in a given droplet, the droplet size distribution must be taken into account. That these two sources of spectral inhomogeneity preclude the

observation of the shell oscillation resonances, can be reliably established.

The spectrum of the shell oscillations can be well approximated as the Fourier transform of the time correlation of the density, $c(t) = \langle \delta\rho(0)\delta\rho(t) \rangle$, in which $\delta\rho(0)$ is the suddenly created compression density at the interface by the optical excitation. For concentric bubble and droplet, the correlation function is periodic, with period determined by the recursion time of the density packet reflected between the two boundaries ($\tau = 2d/v$). For an eccentric bubble, there will be dispersion in recurrence times, given by the distribution of path lengths L_i of re-entrant rays that originate from the bubble wall. We use ray-tracing to compute path lengths of partial waves radiating at angle θ , as a function of displacement of the molecule from the droplet center ε , for a given droplet of radius R and bubble radius r , to obtain the recursion times $\tau_i(\theta, \varepsilon) = L_i(\theta, \varepsilon)/v$, where v is the speed of sound (see inset to Fig. 5). The time-correlation function is then constructed as

$$c(t) = \frac{1}{2} \sum_i \int_0^{R-r} d\varepsilon P(\varepsilon) \int_0^\pi d\vartheta \sin\vartheta g(t - \tau_i(\vartheta, \varepsilon)), \quad (4)$$

in which $g(t)$ is a Gaussian of width $\delta/v = 5$ ps, corresponding to the reflection time of a phonon packet of width $\delta = 5$ Å consistent with the TDFD compression width seen in Fig. 2. The normalized probability of a given displacement, $N\varepsilon^2 \exp(-V(\varepsilon)/kT)$, is dictated by the potential energy experienced by the impurity in a droplet. For the latter, we use the construct of potentials given by Lehmann for ionic [19] and neutral impurities

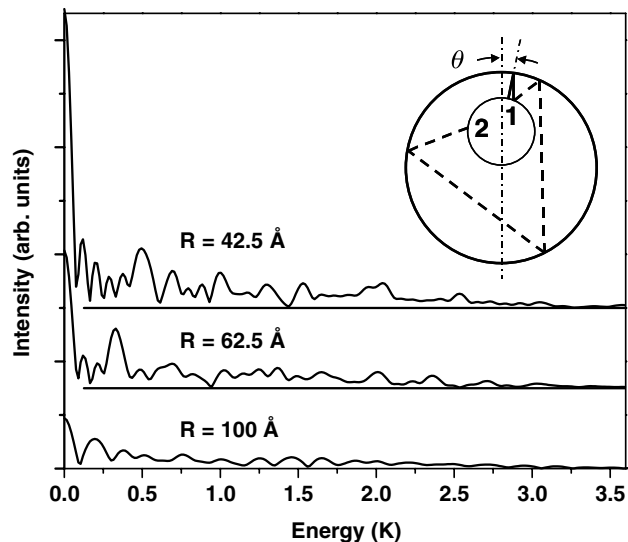


Fig. 5. Shell oscillation spectra for a neutral impurity trapped in droplets of radius $R = 42.5$, 62.5 and 100 Å, including the thermal distribution of eccentricity of the impurity. The spectra are calculated by tracing the recursion of partial waves reflected between the bubble and droplet boundaries. A ray trace showing the first two recursions is shown in the inset.

[20]. In Fig. 5, we show the resulting spectra for neutral impurities in three different droplet sizes. The broad distribution of eccentricities eliminates overtones, leaving a weak and broadened fundamental resonance shifted from the zero-phonon line by $\bar{\nu} = 0.34, 0.23$ and 0.135 cm^{-1} in droplets of radius 42.5, 62.5 and 100 \AA , respectively. An effective recursion length, $\langle L(R) \rangle = v/\bar{\nu}c$, can be associated with the surviving frequency: $\langle L(R) \rangle = 4.93, 5.05, 5.18 R$, for the three different droplet sizes. Due to the shallow trapping potential, as the droplet size increases, the bubble displacement distribution peaks near the droplet wall. Consistent with this, $\langle L(R) \rangle$ tends to $2\pi R$, indicating that the only periodic recursion that survives is that of the whispering gallery mode. In the case of ionic dopants, the fact that the eccentricity is limited by a tighter potential that is nearly harmonic [19], well-defined spectral progressions develop in the larger bubbles. However, these frequencies are rather sensitive to the size of the droplet, and the inclusion of the broad droplet distributions encountered in experiments [1], eliminates all sharp spectral features. The spectra will be further degraded by homogeneous broadening, due to the thermal population of surface excitations (ripples), and energy imparted to the droplet during pick-up of impurities, which has been neglected in the present treatment.

4. Conclusions

We have presented a method for direct dynamical calculations of electronic absorption spectra for molecules embedded in superfluid ^4He . The calculations provide insight into the phonon wing structure, and connect spectral features to the underlying microscopic dynamics of the liquid. We have considered an idealized system, subject to spherical symmetry, initially at 0 K. Nevertheless, the calculations capture the essence of the physics that must govern experimental observations. We reproduce the 9 and 14 K phonon sidebands observed both in helium droplets and in bulk helium [2,3]. Indeed, these peaks correspond to the extrema in the phonon dispersion curve of superfluid helium. The dynamical analysis identifies them as persistent interfacial motion, due to the stationary phonons localized at the guest site. In the dynamical picture, the fact that the peaks occur at the dispersion curve extrema is associated with the zero group velocity of phonons, rather than the increase in the density of states. Indeed, these bands gain intensity when the liquid is further localized through dispersive molecule–helium interactions. Otherwise, on strictly repulsive potentials, the most prominent feature is the liquid breathing mode, which occurs at a much lower frequency, 1–2 K above the zero-phonon line. This motion has been studied through real-time measurements [21]. In finite size

droplets, the harmonic progression of shell vibrations ($\omega = 2\pi\nu/2d$) appear in the gap between the zero-phonon line and the atom evaporation limit of 7 K. The regular sharp progression observed in the TDFT simulation, is limited to impurities trapped at the center of the droplet. The eccentricity distribution in a given droplet size, and the droplet size distribution in experimental realizations, nearly completely destroy the visibility of such resonances. Sharp lines are observed in the same gap region, in a variety of droplet spectra, including the well-analyzed cases of glyoxal and tetracene, which have been suggested to arise from vibrations of highly localized helium atoms [22]. Our analysis supports this suggestion, which otherwise is based on calculations in small clusters ($N < 20$) with strong guest–helium van der Waals binding, $\sim 100 \text{ K}$ [23]. Although broadened by inhomogeneous contributions, shell vibrations must be present in all optical spectra recorded in large droplets.

Acknowledgements

Computational resources provided by the Finnish Center for Scientific Computing (CSC) are gratefully acknowledged. This research was supported in part through a Grant from the NSF (0317138).

References

- [1] J.P. Toennies, A.F. Vilesov, *Annu. Rev. Phys. Chem.* 49 (1998) 1.
- [2] Q. Hui, M. Takami, *J. Low Temp. Phys.* 119 (2000) 393.
- [3] M. Hartmann, F. Mielke, J.P. Toennies, A.F. Vilesov, G. Benedek, *Phys. Rev. Lett.* 76 (1996) 4560.
- [4] M. Hartmann, M. Lindinger, J.P. Toennies, A.F. Vilesov, *Chem. Phys.* 239 (1998) 139.
- [5] S. Grebenev, M. Hartmann, A. Lindinger, N. Pörtner, B. Sartakov, J.P. Toennies, A.F. Vilesov, *Physica B* 280 (2000) 65.
- [6] F. Stienkemeier, A.F. Vilesov, *J. Chem. Phys.* 115 (2001) 10119.
- [7] A. Lindinger, J.P. Toennies, A.F. Vilesov, *Phys. Chem. Chem. Phys.* 3 (2001) 2581.
- [8] M. Hartmann, A. Lindinger, J.P. Toennies, A.F. Vilesov, *Phys. Chem. Chem. Phys.* 4 (2002) 4839.
- [9] J. Eloranta, V.A. Apkarian, *J. Chem. Phys.* 117 (2002) 10139.
- [10] F. Dalfovo, A. Lastri, L. Pricapenko, S. Stringari, J. Treiner, *Phys. Rev. B* 52 (1995) 1193.
- [11] M. Casas, F. Dalfovo, A. Lastri, L. Serra, S. Stringari, *Z. Phys. D* 35 (1995) 67.
- [12] L. Lehtovaara, T. Kiljunen, J. Eloranta, *J. Comput. Phys.* 194 (2004) 78.
- [13] L. Giacomazzi, F. Toigo, F. Ancilotto, *Phys. Rev. B* 67 (2003) 104501.
- [14] P.W. Anderson, *Phys. Rev.* 86 (1952) 809.
- [15] J. Eloranta, N. Schwentner, V.A. Apkarian, *J. Chem. Phys.* 116 (2002) 4039.
- [16] N. Pörtner, J. Peter Toennies, A.F. Vilesov, *J. Chem. Phys.* 117 (2002) 6054.

- [17] J. Eloranta, Preliminary CCSD(T)/AVTZ calculations, unpublished.
- [18] J. Dupont-Roc, M. Himbert, N. Pavloff, J. Treiner, *J. Low Temp. Phys.* 81 (1990) 31.
- [19] K.K. Lehmann, J.A. Northby, *Mol. Phys.* 97 (1999) 639.
- [20] K.K. Lehmann, *Mol. Phys.* 97 (1999) 645.
- [21] A.V. Benderskii, J. Eloranta, R. Zadoyan, V.A. Apkarian, *J. Chem. Phys.* 117 (2002) 1201.
- [22] P. Huang, K.B. Whaley, *Phys. Rev. B* 67 (2003) 155419.
- [23] P. Hobza, O. Bludsky, H.L. Selzle, E.W. Schlag, *J. Chem. Phys.* 97 (1992) 335.